

Comparison of the *COBE*¹ FIRAS and DIRBE Calibrations

D.J. Fixsen^{2,6}, J.L. Weiland², S. Brodd², M.G. Hauser³, T. Kelsall⁴, D.T. Leisawitz⁵, J.C. Mather⁴, K.A. Jensen², R.A. Shafer⁴, R.F. Silverberg⁴

ABSTRACT

We compare the independent FIRAS and DIRBE observations from the *COBE* in the wavelength range 100-300 μm . This cross calibration provides checks of both data sets. The results show that the data sets are consistent within the estimated gain and offset uncertainties of the two instruments. They show the possibility of improving the gain and offset determination of DIRBE at 140 and 240 μm .

Subject headings: cosmology: cosmic microwave background — cosmology: observations — infrared: general — instrumentation: photometer, spectrograph

1. Introduction

The measurement of the sky brightness with the Far InfraRed Absolute Spectrophotometer (FIRAS) and the Diffuse InfraRed Background Experiment (DIRBE) instruments (Boggess *et al.* 1992; Mather *et al.* 1993; Silverberg *et al.* 1993) provides important information on the infrared sky. The two instruments were both designed to determine all-sky absolute brightness, but calibrations of these instruments were done in different and independent ways. FIRAS is a spectrometer, and DIRBE a broad-band photometer; their measurements overlap in the wavelength range 100 - 300 μm . A natural question is: “do these two very different instruments find the same results where their measurements overlap?” Comparison of the two provides a check on the accuracy of the sky measurements.

¹The National Aeronautics and Space Administration/Goddard Space Flight Center (NASA/GSFC) is responsible for the design, development, and operation of the Cosmic Background Explorer (*COBE*). Scientific guidance is provided by the *COBE* Science Working Group. GSFC is also responsible for the development of the analysis software and for the production of the mission data sets.

²Hughes STX Corporation, Code 685.9, NASA/GSFC, Greenbelt MD 20771.

³Space Telescope Science Institute, 3700 San Martin Drive, Baltimore, MD 21218.

⁴Code 685, NASA/GSFC, Greenbelt MD 20771.

⁵Code 631, NASA/GSFC, Greenbelt MD 20771.

⁶e-mail: fixsen@stars.gsfc.nasa.gov

The FIRAS utilizes a polarizing Fourier-transform spectrometer to measure the difference in radiation from two inputs. One input is connected to an internal blackbody, the other is connected to either the sky or an external blackbody calibrator. The FIRAS derives its absolute calibration from the temperature controlled external blackbody that completely fills the input sky horn. In nine calibration events (approximately one each month) over the 10 month mission the external blackbody was placed into the mouth of the horn. Then over the course of several days the temperature was varied from 2.2K to 20K. There were also eight calibrations where the external calibrator was kept cold. For the cold data ($T_x \sim 2.7$ K), the radiation was essentially zero at frequencies 30 to 100 cm^{-1} (300 to 100 μm) and so allows determination of instrumental offsets. The high temperature data ($T_x \sim 20$ K) then allow determination of the gain. The systematic offset uncertainties of the FIRAS can be calculated from the “PEP” uncertainties (FIRAS Explanatory Supplement; Fixsen *et al.* 1994b). The systematic gain uncertainties from the calibration model itself are $\sim 0.2\%$. However, there are inaccuracies in the bolometer model that lead to larger errors. Comparing the various channels (four detectors and two modes of operation) leads to estimates of $\sim 0.5\%$ for the gain uncertainty. As there is the possibility that the error in the bolometer model could bias all of the detectors in the same direction, we use a conservative estimate of the uncertainty of 2% for the high frequency FIRAS data (20-80 cm^{-1}). At the highest FIRAS frequencies (80-100 cm^{-1}), the uncertainty on the temperature of the external blackbody during calibration increases the gain uncertainty exponentially with frequency as this is on the Wein side of the Planck function. The gain has been verified at lower frequencies to 0.5% by comparison with data from the COBE/DMR experiment (Fixsen *et al.* 1994a).

The DIRBE is an absolute radiometer, which measures sky brightness by chopping between the sky and a zero-flux internal reference at 32 Hz. Instrumental offsets were measured roughly five times per orbit by closing a cold shutter located at the prime focus. A constant radiative offset signal in the long-wavelength detectors was found to originate from the JFET amplifiers operating at about 55 K within the dewar. This offset was measured via the shutter-closed calibrations and removed from the data; systematic uncertainty in the offset correction is approximately 160, 250 and 30 kJy/sr at 240, 140, and 100 μm respectively (DIRBE Explanatory Supplement, 1997). Relative gain stability of $\sim 1\%$ was achieved over the course of the mission by frequently monitoring internal radiative reference sources and isolated bright celestial sources. Measurements were placed on an absolute photometric scale through the use of Voyager observations and atmospheric models of Jupiter (140 and 240 μm) and Uranus (100 μm). The uncertainty in the absolute gain at these wavelengths is $\sim 10\%$ (DIRBE Explanatory Supplement, 1997).

2. The Data

FIRAS and DIRBE data are pixelized into maps using a common projection and coordinate system (geocentric ecliptic coordinates, epoch 2000). The projection, referred to as the quadrilateralized sphere (O’Neill & Laubscher, 1976; DIRBE Explanatory Supplement, 1997),

approximately preserves area. The FIRAS and DIRBE pixels are related such that there are 64 DIRBE pixels for every FIRAS pixel. Full FIRAS coverage of the sky is given in 6144 pixels; DIRBE has 393216 pixels.

The high frequency FIRAS “Pass 4” data consist of 167 point spectra between 20 and 100 cm^{-1} ($500 \mu\text{m}$ to $100 \mu\text{m}$) in each of 6067 pixels on the sky (77 pixels have no data). They were calibrated using the method described in Fixsen *et al.* 1994b, with the improvements noted in Fixsen *et al.* 1996. A weighted average of all of the high frequency FIRAS data was used. The weights and uncertainties are discussed in Fixsen *et al.* 1994b.

For the DIRBE counterpart to the FIRAS data, we used the DIRBE $240 \mu\text{m}$, $140 \mu\text{m}$ and $100 \mu\text{m}$ (bands 10, 9 and 8) “Annual Average Maps” from the 1997 Pass 3b production software release. “Annual Average Maps” are weighted averages of the first 10 months of data taken during the cryogenic period (11 Dec 1989 to 21 Sep 1990); these maps are described in the DIRBE Explanatory Supplement (1997). Random uncertainties associated with the DIRBE measurements are also taken from the Annual Average product; these are the standard deviations of the photometric mean reported for each pixel. The use of the Annual Average Maps is essential for the band 10 and 9 comparisons, since many observations are needed to achieve the best DIRBE signal-to-noise ratio possible at these wavelengths in dark parts of the sky. However, since FIRAS sky measurements are all made at a solar elongation, e , of 94° , there is an error introduced by comparing the FIRAS dataset with the DIRBE Annual Average Maps, which sample a mix of solar elongation angles for each pixel. The error is wavelength dependent and diminishes with increasing wavelength, as it is the emission from the interplanetary dust cloud which introduces the discrepancy. At $100 \mu\text{m}$, the $1\text{-}\sigma$ photometric error associated with using the Annual Average Map rather than a map interpolated to $e = 94^\circ$ is $\sim 3\%$ (of order 100 kJy/sr at the Galactic poles). Darker regions ($|b| > 30^\circ$), where zodiacal emission can contribute up to 60-70% of the observed sky brightness, are more affected than the Galactic plane. As will be seen in section 3, the use of the Annual Average band 8 map, while not ideal, is not the limiting uncertainty in the comparison with the FIRAS data. At 140 and $240 \mu\text{m}$, emission from the Galaxy dominates over that from the interplanetary dust at nearly all latitudes, and the band 9 error associated with using the Annual Average is estimated as $< 1\%$ ($\sim 40 \text{ kJy/sr}$) at high Galactic latitudes, and completely negligible for all parts of the sky in band 10.

3. Data Preparation

Before comparing the FIRAS and DIRBE maps, the data must be converted to a common spectral and spatial format. The spectral information of the FIRAS is converted into a broadband photometric measurement like the DIRBE’s, and the DIRBE spatial resolution is degraded to that of the FIRAS.

3.1. FIRAS

For each 3° FIRAS pixel, the high frequency spectral data, $I_F(\nu)$, are convolved with the DIRBE system responsivity, $R_D(\nu)$ (see fig 1), in order to produce two maps to compare to DIRBE bands 9 and 10. Since DIRBE flux densities are quoted in each passband using an assumed intrinsic spectral energy distribution $\nu I_\nu = \text{constant}$, we use the following equation to compute the corresponding FIRAS brightness in each pixel:

$$I_F^{\nu_0} = \frac{\int I_F(\nu)R_D(\nu)d\nu}{\int \frac{\nu_0}{\nu}R_D(\nu)d\nu} \quad (1)$$

where ν_0 is the frequency corresponding to the DIRBE nominal wavelength, and integration covers the passband.

Special treatment is required for the DIRBE band 8, as the FIRAS spectral data do not extend to the short-wavelength edge of the DIRBE passband. We construct an alternate truncated passband over which the FIRAS data may be integrated, and then use a “color correction” factor to derive the equivalent value for the true DIRBE passband. We consider two truncated passbands, $R_{8x}(\nu)$. The first, $R_{8'}(\nu)$, uses a spectrum tuned to the FIRAS noise, and has a lower mean frequency (and hence a larger color correction). The second passband, $R_{8''}(\nu)$, is a better match to the DIRBE band 8, but weights frequencies for which the FIRAS data have higher intrinsic noise. Both $R_{8'}(\nu)$ and $R_{8''}(\nu)$ are plotted in figure 1 to show the relationship to the actual DIRBE 100 μm bandpass.

The calculation of the color correction is dependent upon the contributors to the sky flux in the bandpass. Since both zodiacal and Galactic emission are important contributors at wavelengths near 100 μm , we rewrite the observed FIRAS sky brightness $I_F(\nu)$ as the sum of “zodiacal” and “non-zodiacal” terms:

$$I_F(\nu) = Z(\nu) + [I_F(\nu) - Z(\nu)], \quad (2)$$

where the term in square brackets is expected to be dominated by Galactic emission. The FIRAS band 8 map is then computed using

$$I_F^{\nu_0} = C_{8x}^Z \frac{\int [Z(\nu)]R_{8x}(\nu)d\nu}{\int \frac{\nu_0}{\nu}R_{8x}(\nu)d\nu} + C_{8x}^{I-Z} \frac{\int [I_F(\nu) - Z(\nu)]R_{8x}(\nu)d\nu}{\int \frac{\nu_0}{\nu}R_{8x}(\nu)d\nu} \quad (3)$$

where C_{8x}^Z and C_{8x}^{I-Z} are color corrections appropriate to each component. We use the DIRBE interplanetary dust model (Reach *et al.* 1996; Kelsall *et al.* 1997) to evaluate the zodiacal contribution $Z(\nu)$.

To compute the color corrections C_{8x} , we assume that each of the two sky components may be approximated with a spectrum of form $\alpha\nu^\beta B(T, \nu)$ where α , β and T are parameters of the fit and $B(T, \nu)$ is the Planck function. The color correction is then estimated as:

$$C_{8x} = \frac{\int \nu^\beta B(T, \nu)R_D(\nu)d\nu}{\int \nu^\beta B(T, \nu)R_{8x}(\nu)d\nu} \quad (4)$$

To determine the spectral model for the $(I - Z)$ component we subtracted the DIRBE model of the zodiacal emission, Z , from the FIRAS emission, then estimated the temperature and index of the remaining average spectrum over the entire sky (G) or only over the $|b| > 20^\circ$ region (H). The parameters of the spectrum fits are: $(\beta, T)=(1.72, 19.9), (1.54, 19.6)$ and $(.6, 116)$ for the full sky (G), high latitude sky (H) and the zodiacal model respectively. These give color corrections of .78, .74 and 2.19 for the $8'$ passband and .83, .81 and 1.5 for the $8''$ passband. The spectral variation of different sources gives rise to a range of color corrections. The color corrections given here are reasonable, but variations of $\sim 10\%$ over the sky or under other assumptions are possible.

3.2. DIRBE

The FIRAS data have $\sim 7^\circ$ angular resolution, as measured by their full width at half maximum (FWHM), but the DIRBE beam profiles are $\sim 0.7^\circ$. To compare these two data sets, the DIRBE data were convolved with a map of the FIRAS beam obtained from on orbit data taken when the moon was near the FIRAS beam (See Fig 2). The COBE rotates about the optical axis of the FIRAS instrument, so *on average* the beam must have cylindrical symmetry. However, the time it takes to collect a single interferogram is less than a rotation period, so a particular measurement beam may be asymmetric. The dwell time for each FIRAS interferogram also causes the beam to be elongated in the scan direction by 2.4° . To account for this, the DIRBE data were further convolved one FIRAS pixel (2.6°) along ecliptic meridians (close to the FIRAS scan direction). The convolved DIRBE map data were then decimated to obtain three 6144 pixel all sky maps at the same resolution as the FIRAS data. We estimate that the assumption of beam symmetry may produce residual beam shape errors of order 5%. These errors are only important in the high gradient regions near the Galactic plane.

The mean position of the FIRAS data is not centered within each pixel. While this is a minor matter in the high Galactic latitude regions, near the plane it has a significant effect. To correct for this effect we fit a general second order polynomial (six parameters) to each pixel and its eight closest neighbors on the DIRBE maps after beam convolution and reduction to FIRAS resolution. The difference between the value of this polynomial at the mean location of the FIRAS data and the value at the pixel center is the “gradient correction”. The “gradient correction” was applied to the DIRBE data for each pixel. A typical correction (rms) is 5%.

4. Comparison

Figure 3 presents plots of the FIRAS vs. DIRBE data after the data conversion steps described above. There is a clear correlation between the measurements in all 3 bands. The noise appears higher in the FIRAS data than in the DIRBE data: part of this is due to the larger variation in the FIRAS sky coverage, which leaves some pixels with very few observations and hence large

errors.

We make a formal fit

$$I_F = gI_D + o, \tag{5}$$

with free gain g and offset o parameters, to fit the FIRAS data to the DIRBE data for each DIRBE band. Our first set of fits allowed only for the random errors in the DIRBE and FIRAS data; the results for these are presented in Table 1 and are indicated with an asterisk. The results are encouraging but the formal χ^2 is large: a problem is evident in regions of high gradient.

The beam shape and the gradient correction errors might account for the large χ^2 , but the residual DIRBE gain uncertainties and residual stripes in the FIRAS data might also be significant. To account for these, we include in the uncertainty estimate 5% for the beam error and a 0.5° gradient correction error. Both sets of statistics are included in Table 1 to show how these affect the gain and offset determination between the instruments. We include fits over the entire sky, which are listed in Table 1 as the results for a Galactic cut of 0° . Alternatively, we can restrict our comparison to the high Galactic latitude regions ($|b| > 10^\circ$ or 20°). This reduces the available dynamic range over which to compare the gains, but also acts to reduce the biases in the derived offset.

Quadratic fits of the form $I_F = qI_D^2 + gI_D + o$ are included to test the linearity of the instruments. Since the brightest part of the sky is $\sim 10^6$ kJy/sr, the fifth column in Table 1 gives an estimate of the fraction of the nonlinearity over the full range. The Galactic plane is needed to give a good estimate for the quadratic parameter.

5. Discussion

There are several issues that are apparent from the results listed in Table 1. The statistical uncertainties listed there are clearly not the major uncertainty in comparing the two data sets. The difference in the fits with and without the Galactic plane is consistently a larger factor. This might be a problem with detailed pointing, beam shape problems, color variation differences coupled with errors in the response function, or variation in zodiacal emission. All of these problems are larger at higher frequency and many of them are larger in the Galactic plane.

Even with these limitations, for DIRBE bands 10 and 9, there is no evidence for non-linearity: the gain ratio can be determined to within a percent or so, and the offset can be roughly determined. For the gain ratio and quadratic term, the estimates including the Galactic plane are better, because they have a much longer lever arm, as indicated by the statistical uncertainties. Still, the variation when the Galactic plane is excluded should not be ignored, but used as evidence of the real uncertainty of the comparison. To find the offset between the measurements, removing the Galactic plane eliminates many of the problems and uncertainties of the comparison as indicated by the χ^2 but leaves 2/3 of the sky to compare. Again, the differences between the

other fits are an indicator of the real uncertainty.

The comparison between FIRAS and DIRBE band 8 has all of the caveats of the comparison to bands 9 and 10, plus those associated with the “color” correction. Many other schemes for comparing the FIRAS data with the DIRBE band 8 data are possible; the methods shown here are only meant to convey the range of solutions that result from reasonable sorts of fits. We note that there is an inconsistency in tabulating all-sky fits for the high-latitude (H) solutions, and similarly in showing fits to data cut at $b = 20^\circ$ for the all-sky (G) solutions. However, we include these within Table 1 to show that the dominant effect is that of latitude cut rather than color correction. We adopt a similar philosophy for the entries in which the data have been cut at $b = 10^\circ$, but color corrected to match either the G or H solutions. The high χ^2 obtained for the $100 \mu\text{m}$ fits is a reminder that there are still problems. The extrapolation has the intrinsic problem that any emission beyond 97 cm^{-1} cannot be observed by the FIRAS instrument.

In addition to the random uncertainties and the uncertainties generated in the process to obtain comparable data, there are the systematic uncertainties associated with each instrument. While the random uncertainties are lower in the DIRBE data, the FIRAS calibration is done directly to a temperature-controlled blackbody source, and this provides the FIRAS with lower absolute uncertainties in gain and offset.

6. Conclusions

After examining the fits in Table 1 and other permutations on fitting options, we note the uncertainties are not dominated by the statistical uncertainties but by other effects. We have adopted values for the gain and offset based upon results from those fits in Table 1 which are best suited for determining these parameters. For band 8, this means the $8''$ bandpass is probably better because it is a closer frequency match. The offsets were selected from the fits excluding the galactic plane, including comparison uncertainties. The gains were chosen from fits including the Galactic plane and comparison uncertainties. The final results, uncertainties and upper limits for a quadratic effect are summarized in Table 2. The uncertainties are the dispersion in the results from Table 1. They are dominated by systematic effects in the comparison rather than the intrinsic noise, but the results still test the DIRBE calibration.

The FIRAS spectra convolved with the DIRBE pass bands agrees with the DIRBE observations convolved with the FIRAS beam within the estimated DIRBE uncertainties. This lends support to the stated DIRBE uncertainties in both the gain and offset. The comparison uncertainties provide a poor check on DIRBE band 8. However, the lower FIRAS systematic uncertainties could be used to recalibrate DIRBE bands 9 and 10 to reduce their systematic uncertainties.

This work was supported by *COBE* Extended Mission funding from the NASA Office of Space Sciences.

Table 1: FIRAS-DIRBE Cross-Calibration Results

Band	Galaxy Cut (degrees)	Offset (kJy/sr)	Gain -	Quadratic (10^{-6} sr/kJy)	χ^2 /DOF -
10*	0	-177 ± 3	1.0600 ± 0.0001	-	472.09
10*	20	-133 ± 5	1.0462 ± 0.0007	-	3.29
10	0	-185 ± 6	1.0566 ± 0.0012	-	1.04
10	10	-165 ± 7	1.0511 ± 0.0015	-	1.21
10	20	-137 ± 8	1.0425 ± 0.0019	-	1.03
10	0	-177 ± 6	1.0546 ± 0.0013	0.04 ± 0.01	1.04
9*	0	-917 ± 15	1.0539 ± 0.0002	-	43.19
9*	20	-509 ± 30	1.0183 ± 0.0031	-	1.61
9	0	-671 ± 24	1.0408 ± 0.0018	-	1.39
9	10	-627 ± 29	1.0344 ± 0.0028	-	1.70
9	20	-515 ± 36	1.0174 ± 0.0043	-	1.39
9	0	-647 ± 26	1.0379 ± 0.0022	0.02 ± 0.01	1.39
8' _G *	0	-1596 ± 36	1.2414 ± 0.0005	-	11.55
8' _G *	20	-196 ± 56	1.0416 ± 0.0068	-	1.58
8' _G	0	-1483 ± 35	1.2381 ± 0.0028	-	1.89
8' _G	10	-834 ± 51	1.1463 ± 0.0055	-	2.00
8' _G	20	-305 ± 61	1.0564 ± 0.0077	-	1.51
8' _G	0	-1465 ± 40	1.2358 ± 0.0037	0.02 ± 0.02	1.89
8' _H *	0	-1323 ± 22	1.1779 ± 0.0005	-	11.50
8' _H *	20	-123 ± 54	1.0066 ± 0.0065	-	1.57
8' _H	0	-1244 ± 34	1.1777 ± 0.0028	-	1.82
8' _H	10	-703 ± 48	1.1006 ± 0.0053	-	1.95
8' _H	20	-255 ± 58	1.0251 ± 0.0073	-	1.49
8' _H	0	-1239 ± 38	1.1771 ± 0.0036	0.00 ± 0.02	1.82
8'' _G *	0	-2693 ± 124	1.3100 ± 0.0028	-	3.07
8'' _G *	20	54 ± 299	1.0210 ± 0.0361	-	2.46
8'' _G	0	-1801 ± 134	1.2495 ± 0.0054	-	2.59
8'' _G	10	-265 ± 243	1.0909 ± 0.0248	-	3.11
8'' _G	20	74 ± 302	1.0181 ± 0.0365	-	2.45
8'' _G	0	-557 ± 158	1.1289 ± 0.0098	0.40 ± 0.03	2.55
8'' _H *	0	-2542 ± 121	1.2785 ± 0.0027	-	3.07
8'' _H *	20	80 ± 292	1.0046 ± 0.0352	-	2.46
8'' _H	0	-1660 ± 131	1.2187 ± 0.0054	-	2.58
8'' _H	10	-208 ± 238	1.0690 ± 0.0243	-	3.11
8'' _H	20	100 ± 294	1.0019 ± 0.0357	-	2.45
8'' _H	0	-464 ± 155	1.1024 ± 0.0096	0.39 ± 0.03	2.54

* These fits use the random uncertainties of the FIRAS and DIRBE data only.

The 8' and 8'' passbands use different extrapolations of the FIRAS data to compare to the DIRBE data.

GH The 8_G and 8_H use different color corrections of the FIRAS data to compare to the DIRBE data. See text.

Table 2. Adopted FIRAS-DIRBE Calibration

DIRBE Band	Offset kJy/sr	Gain -	Quadratic limits 10^{-6} sr/kJy
10	$-137 \pm 22 \pm 20$	$1.06 \pm 0.01 \pm 0.02$	0.05
9	$-515 \pm 150 \pm 120$	$1.04 \pm 0.02 \pm 0.02$	0.04
8	$100 \pm 830 \pm 900$	$1.25 \pm 0.10 \pm 0.15$	0.2

Uncertainties are dominated by systematic effects. Second uncertainties are the absolute uncertainties of the FIRAS data.

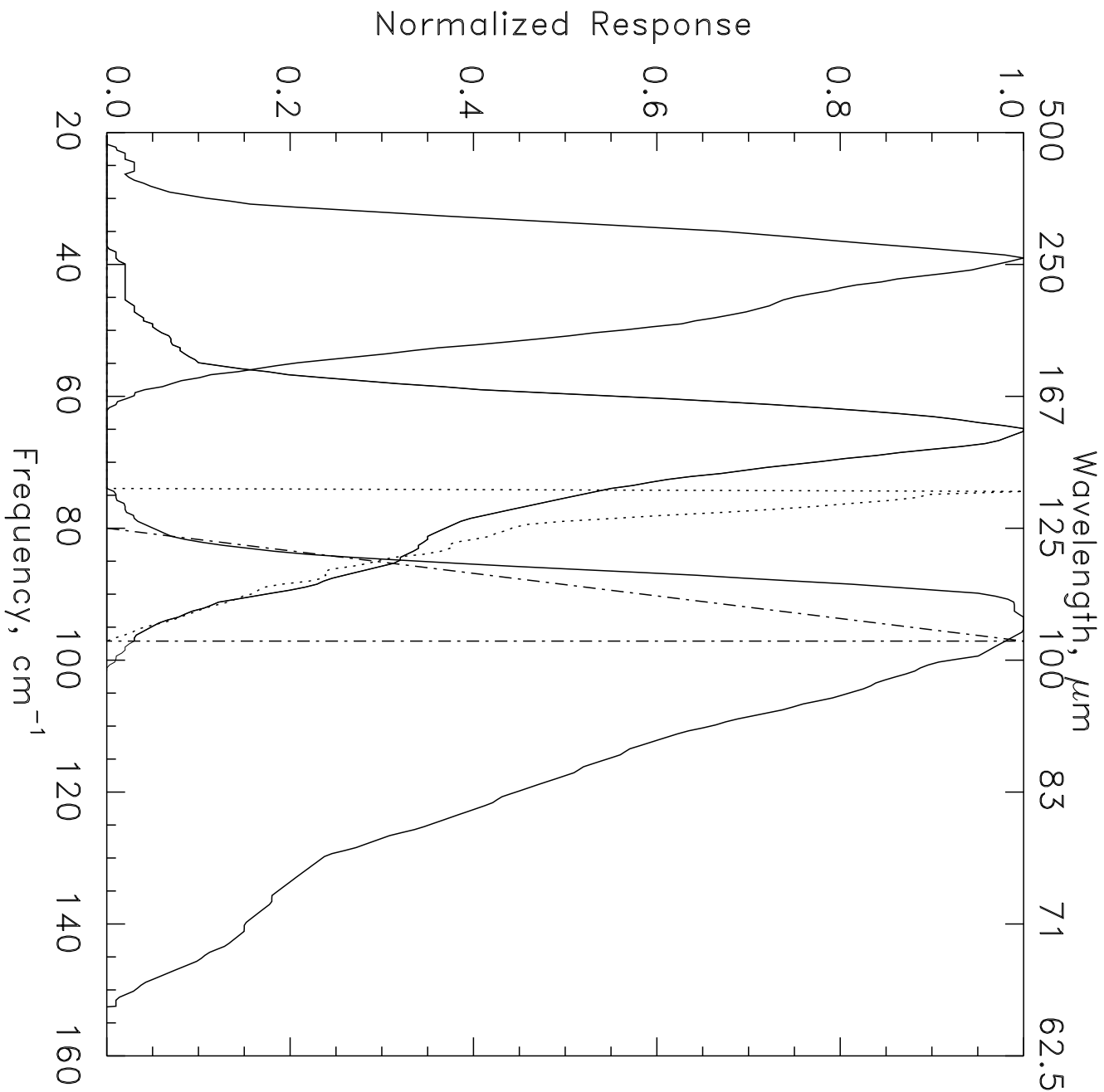
REFERENCES

- Bennett, C. L. *et al.* , 1996, ApJ, 464, L1
- Boggess, N. W. *et al.* , 1992, ApJ, 397, 420
- COBE Diffuse Infrared Background Experiment (DIRBE) Explanatory Supplement*, ed. M. G. Hauser, T. Kelsall, D. Leisawitz, and J. Weiland, *COBE* Ref. Pub. No. 97-A (Greenbelt, MD: NASA/GSFC), available in electronic form from the NSSDC.
- COBE Far Infrared Absolute Spectrometer (FIRAS) Explanatory Supplement*, ed. J.C. Mather, R.A. Shafer, R.E. Eplee, D.J. Fixsen, R.B. Isaacman and A.R. Trenholme, *COBE* Ref. Pub. No. 95-C (Greenbelt, MD: NASA/GSFC), available in electronic form from the NSSDC.
- Fixsen, D. J. *et al.* , 1994a, ApJ, 420, 445
- Fixsen, D. J. *et al.* , 1994b, ApJ, 420, 457
- Fixsen, D. J. *et al.* , 1996, ApJ, 473, 576
- Kelsall, T., *et al.* , 1997, *in preparation*
- Mather, J.C., Fixsen, D.J. and Shafer, R.A. “Design for the COBE Far Infrared Absolute Spectrophotometer (FIRAS),” COBE Preprint 93-10, Proc. SPIE, vol 2019, pp. 168-179, conf. on Infrared Spaceborne Remote Sensing, in San Diego, CA, 11-16 July 1993, (SPIE: Bellingham, WA)
- O’Neill, E. M. & Laubscher, R. E. 1976, Extended Studies of a Quadrilateralized Spherical Cube Earth Data Base, (NEPRF Technical Report 3-76) (NTIS Report AD-A026294) (Computer Sciences Corp. CSC/TR-76/6008)
- Reach, W.T., Franz, B.A., Kelsall, T. and Weiland, J.L., 1996, in “Unveiling the Cosmic Infrared Background”, ed. E. Dwek, (AIP: New York), pp. 37
- Silverberg, R. F., *et al.* , 1993, Proc. SPIE Conf. 2019, “Infrared Spaceborne Remote Sensing”, ed. M.S. Scholl (SPIE: Bellingham), pp. 180

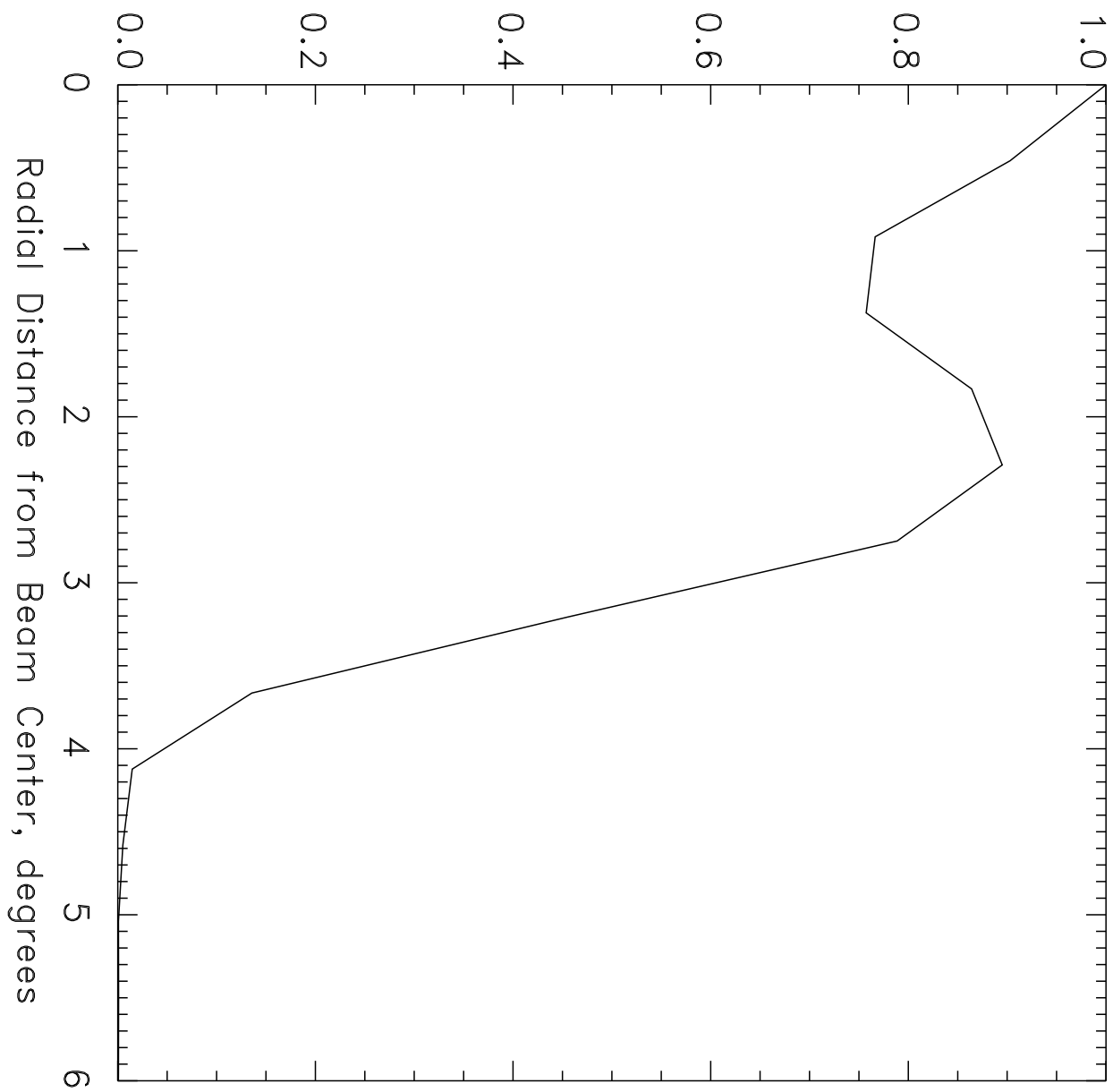
Fig. 1.— DIRBE passbands and FIRAS approximations to DIRBE band 8. The DIRBE 10, 9 and 8 bands are plotted as solid lines. The $8'$ and $8''$ band constructs are plotted as dotted and dot-dash lines, respectively. The $8'$ and $8''$ approximations are necessary because the FIRAS data ends at 97 cm^{-1} ; the truncation has an insignificant effect on band 9. Color corrections must be applied to band 8 results.

Fig. 2.— FIRAS Beam response as function of angle from central axis.

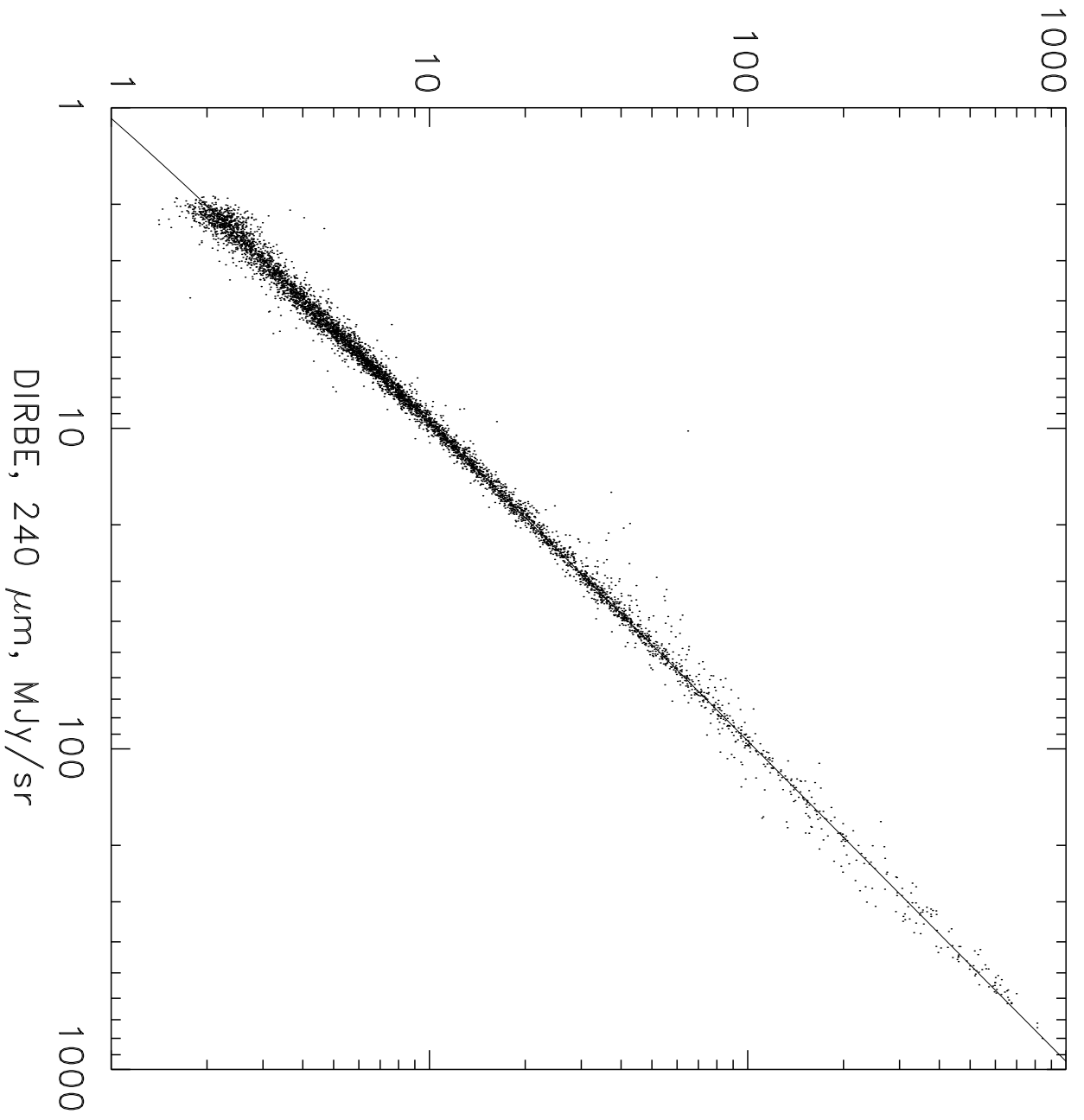
Fig. 3.— Scatter plots of the DIRBE data vs the FIRAS data, after conversion to a common format. The solid line corresponds to the adopted fit given in Table 2. a) $240\ \mu\text{m}$ (Band 10) b) $140\ \mu\text{m}$ (Band 9) c) $100\ \mu\text{m}$ (Band 8, using the $8''$ bandpass).



Normalized FIRAS Beam Response



FIRAS, 240 μm , MJy/sr



FIRAS, 140 μm , MJy/sr

